

A Highly Sensitive Surface-Modified Porous Carbon Nanotube-Based Sensor for Ammonia Gas Detection

Shah Masheerul Aalam, Mohd Sarvar, Mohd Sadiq, and Javid Ali*

Cite This: *ACS Omega* 2024, 9, 4486–4496

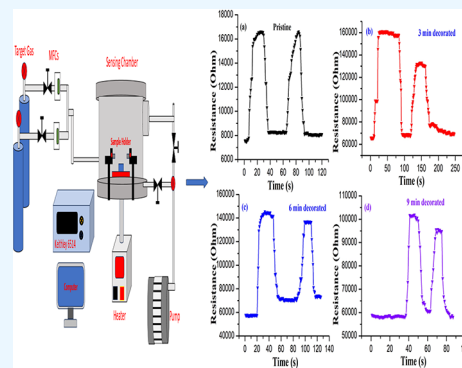
Read Online

ACCESS |

Metrics & More

Article Recommendations

ABSTRACT: In this work, we compared the gas sensing behaviors of pristine and decorated multi-walled carbon nanotubes (MWCNTs) and examined the response behavior of bare and adorned MWCNTs in gas sensing. According to the data, the decorated response was 144%, which is higher than the bare CNT response of 117% in terms of the sensing response. The RF-sputtering method is used to decorate the carbon nanotubes by pure Indium (In) metal nanoparticles. Every measurement was performed in a temperature-controlled environment. Tests of the entire procedure were conducted at a 10 ppm concentration of ammonia gas. We have observed the quick reaction time (1–10 s) in pristine and (1–7 s) in decorated MWCNTs. The response was obtained 117% for the pristine and 144, 115, and 73% for the second (3 min decoration), third (6 min decoration), and fourth (9 min decoration) MWCNTs, respectively. The as-prepared pristine samples and all the decorated sensors had sensitivity values of 0.45, 0.50, 0.51, and 0.57 for time intervals of 0, 3, 6, and 9 min, respectively. It amounted to 45% for the pure and 50, 51, and 57% for the remaining as-prepared decorated sensors, respectively. Based on the measured sensor response graph, a recovery of between 80 and 85% was achieved. For a period of 10 days at a constant concentration, the stability was also assessed and we have analyzed the structural, electrical, and elemental composition of the prepared CNTs by FESEM, EDX, Raman spectroscopy, FTIR, and XRD.



1. INTRODUCTION

Living things are in grave danger when hazardous gases and chemicals are released directly into the environment. It is a major worldwide problem that needs to be resolved by taking sensible action. Many poisonous gases can harm your health, even at low levels (ppm or ppb). Effective gas sensors are needed to monitor the level of NH_3 gas in the environment. Conventional gas sensors have a number of major shortcomings, including high operating temperature, large size, and poor efficiency. The identification of gases with higher atmospheric concentrations, such as NH_3 , SO_2 , and H_2O , is made simple by the availability of numerous standard solid-state gas sensors. Many dangerous gases, however, can have concentrations as low as ppm (10^{-6}) or ppb (10^{-9}) in a variety of applications. For an efficient absorption and desorption of analyte gases, conventional solid-state gas sensors require high resistance together with very high operational temperatures (150–250 °C). These elements have an impact on the gas sensor's efficiency and stability. By utilizing various nanomaterials such as metal oxide nanoparticles, carbon nanotubes, and graphene, numerous research groups are devoted to improving the selectivity and sensitivity of gas sensors,^{1–4} etc.

Human health is at risk due to the caustic nature of NH_3 . It specifically damages human eyes, skin, kidneys, liver, and respiratory tract above a concentration of 25 ppm (ppm). Therefore, it is crucial for industrial emission control,

environmental preservation, and human safety to have NH_3 sensing and monitoring. Due to the status of NH_3 as a biomarker for renal and ulcer disorders, NH_3 sensors have recently shown renewed promise in medical applications. Therefore, by measuring the NH_3 content in human breath, NH_3 sensors may be utilized to diagnose various disorders. The average concentration of NH_3 in exhaled breath for a healthy individual is around 0.83 ppm.⁵

Carbon nanotubes and their derivatives are among these materials that have demonstrated enormous potential in this field. Nanostructured materials, such as nanowires, nanobelts, nanotubes, nanorods, and nanofibers, have outperformed other types of sensing layers in terms of stability and surface area, which has increased the quality of the sensing in comparison with bulk materials.^{6–9} Carbon nanotubes (CNTs), which are a graphene derivative used in numerous research disciplines since their discovery, are particularly promising class of nanomaterials.^{10,11} There are numerous methods that can be

Received: September 20, 2023

Revised: November 18, 2023

Accepted: November 30, 2023

Published: January 14, 2024



used to create CNTs at the moment, including chemical vapor deposition (CVD), plasma-enhanced chemical vapor deposition (PECVD), laser ablation plasma-based synthesis, arc discharge evaporation, and thermal synthesis procedure.¹² Moreover, other varieties of CNTs, such as single-walled carbon nanotubes (SWCNTs) and multiwalled carbon nanotubes (MWCNTs), can be produced.^{13,14}

As a result, several researchers have focused heavily on developing gas sensors using techniques other than those that are costly, like gas chromatography.^{15,16} Chemical-resistive sensors are straightforward and have benefits of being transforming into a microsensor;^{17–19} thus, the approach for electrochemical sensors and chemical resistance is appealing, such as a gas sensor employing metal oxides, graphene,^{20–22} and multilayer carbon tubes.^{23–26} Due to their sensitivity to a variety of gases, ability to operate at room temperature, incredibly low detection threshold, and low power requirements, CNT chemical resistance sensors are frequently utilized. Due to their high conductivity and internal gas detecting characteristics, CNTs have been utilized as sensors for chemical resistor-based sensors, which have the benefit of forming a compact sensing system.^{27,28} The efficiency of gas detection may be improved by novel measuring techniques, signal processing, and sensor technology advancements. Recent experimental experiments have shown that the gas sensors' selectivity and sensitivity may be increased by using low-frequency, colored resistance variations induced within them.^{29,30} Temperature modulation of the gas sensing layer is a different technique that may be simply used to enhance gas detection. At low and high operating temperatures, sensitivity decreases as a result of temperature-dependent processes related to gas molecule adsorption and desorption.³¹ It has been demonstrated experimentally, and various temperature profiles should be detected for different gases and used to identify them specifically.^{32,33} When the gas-detecting layer is operating at a high temperature, generally over 150 °C, adsorption and desorption processes are accelerated. However, these circumstances restrict the range of sensor applications and also increase energy usage. The surface of CNTs can be modified with functional groups or metal or metal oxide nanoparticles, which have both been widely employed to enhance gas sensing capability.³⁴

If we discuss the other sensors like photo catalytic materials used for the degradation of formaldehyde to lower the quantity and clean indoor air, the process of adsorption uses the physical and chemical interactions on an adsorbent's surface to accumulate formaldehyde on the adsorbent's surface and pores. The process known as "ionic oxidation" occurs when formaldehyde in the air reacts with negative ions to either settle or change into a harmless molecule. A method called thermal catalytic oxidation uses a catalyst and high temperatures to oxidize and break down dangerous gases. Formaldehyde is most often catalyzed at room temperature by adsorbing it to the air through the use of activated carbon. Photocatalysis technology is used in this experiment. When compared to other methods, photocatalysis boasts easy-to-use equipment and straightforward operation.³⁵

According to Zhou et al.'s experimental findings, the QCM sensor based on CA/PANI/ZnO composite nanomaterials performed well at room temperature over a broad range of ammonia concentrations (1–70 ppm), displaying traits like high linearity, high selectivity, short response recovery times (15 s/10 s), and high sensitivity (4.54 Hz/ppm).³⁶

Fegade et al. worked on mesoporous PbO_x-ZnO nanocomposites, and at ambient room temperature, the device exhibits good selectivity, sensitivity, low detection limit of hydrogen, a response time of 155 s, and a recovery time of 69 s when it is exposed to 5 ppm of H₂ gas.³⁷

On the other hand, defect-induced CNTs are potential sensing layers for gas sensing, and we propose to synthesize them in this work.^{38,39} The CNTs are a viable choice for producing additional interstitial areas and induced flaws. They are therefore appropriate for obtaining a better reaction and higher performance from molecules of the gas. There is a possibility that the defect-induced CNT-based resistive sensor will react reasonably to ammonia gas. The nature of NH₃ molecules' interaction with MWCNTs and the best way to modify pure CNTs for the most effective ammonia detection at low concentrations are the two key issues we address in this work. We used a straightforward and reliable technique to create gas sensor devices that allow for the direct interaction of distinctive MWCNTs with ammonia. Gas sensor devices based on pristine MWCNTs, 3 min decoration nanotubes, 6 min decoration nanotubes, and 9 min decoration nanotubes were all created and thoroughly investigated under identical circumstances. All nanotubes were prepared by a low-pressure chemical vapor deposition method, and the surface was decorated by the RF-sputtering method by indium metal (In) nano particles of the CNTs, which simplifies interpretation of results on the ammonia–CNT interaction. Finally, all measurements were performed at room temperature and the issue of energy efficiency of MWCNT-based ammonia gas sensors was addressed.

As far as the novelty in the current work is concerned, we have not used the heating process for working at elevated temperatures; rather, we have worked at room temperature. Pure indium (In) 99.99% purity metal nanoparticle decoration has been done by the plasma power RF-sputtering method under a vacuum of 10⁻⁶ Torr. The distance between the target and the substrate was about 3 in., the working power was 100 W, the whole process was done under nitrogen gas (N₂) plasma, and the gas flow rate was 50 sccm, which causes the defects and increases the surface area of the sensing layer on the surface, thus enhancing the intrinsic sensitivity toward gas molecules. Thus, we have prepared MWCNTs using the most sophisticated low-pressure chemical vapor deposition technique (LPCVD) using acetylene as the carbon source gas. Ammonia is used for etching the surface, and hydrogen is used as the carrier gas.

2. EXPERIMENTAL DETAILS

First, the N-type silicon substrates were ultrasonically cleaned with acetone for 30 min and then air-dried. Afterward, these Si substrates were put into a muffle furnace to form a SiO₂ layer under the temperature of 1000 °C for 12 h. These prepared SiO₂ substrates were loaded into the RF-sputtering chamber along with an iron (Fe) target mounted on it, with a distance between the target and substrate of around 8 cm, in order to adequately deposit the Fe catalyst. The RF-sputtering chamber was given the necessary vacuum in order to deposit the Fe catalyst in a high-quality manner. High-grade nitrogen (N₂) plasma was created at a power of 100 W under 50 sccm and a deposition pressure of 10⁻⁶.

In the second phase of the experiment, the LPCVD technique was used to generate the MWCNT. The substrates with Fe deposits were added, and the LPCVD chamber was

properly shut. Inside the chamber, a high-quality vacuum of the order of 10^{-3} Torr was produced by a rotary pump that was linked to the system. The pretreatment was followed by an increase in temperature to $750\text{ }^{\circ}\text{C}$. At the ideal temperature of $750\text{ }^{\circ}\text{C}$ and a flow rate of 30 sccm, the carbon source C_2H_2 was injected through the quartz tube, which is horizontally aligned with the heater chamber. Hydrogen and ammonia were also present in the source gas. Ammonia (NH_3) serves as the diluting agent, and hydrogen (H_2) serves as the carrier gas. The breakdown of the Fe catalyst into nanoparticles is evident, and special nanoislands are being formed to encourage the synthesis of MWCNTs. MWCNT formation takes place on these Fe-based nanoislands, and the size of these nanoislands also influences the diameter distribution.

During preparation of the sensor, In metal coating was carried out using the RF-sputtering approach, which can be seen in the schematic diagram in Figure 1, where In

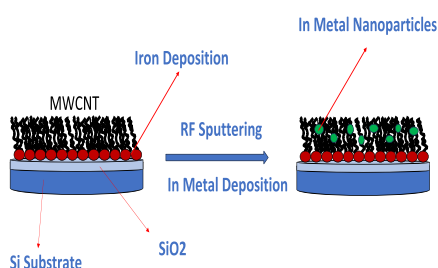


Figure 1. Schematic diagram of metal deposition on MWCNT.

nanoparticles were directly decorated on MWCNT produced by LPCVD on a Si substrate and precoated with the Fe catalyst. During the sputtering process, a target made of In metal that is 99.99% pure is employed. Sputtering has been done in different time intervals like 0 min on pristine, 3 min on sample second, 6 min on sample third, and 9 min on sample fourth. A continuous 100 W of sputtering power was applied at room temperature during the whole operation in the presence of the continuous nitrogen flow of 50 sccm. All throughout the procedure, both the starting and working pressures were 10^{-6} Torr.

A Keithley 6514 source meter is linked to the computer, and data have been recorded. The construction of gas sensing equipment depicted in Figure 2 below has completed all data accusation analysis.

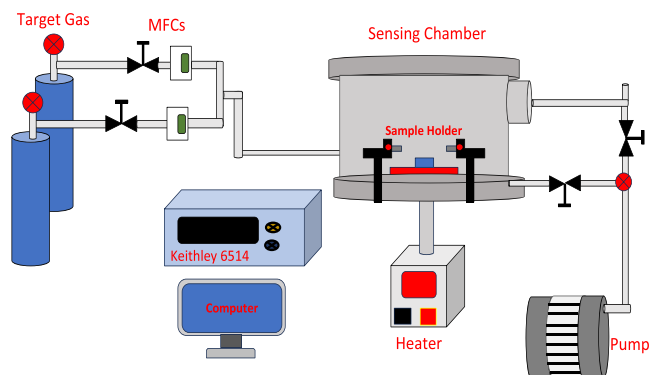


Figure 2. Schematic diagram for the gas sensing and data accusation setup.

3. RESULTS AND DISCUSSION

Field emission scanning electron microscopy (FESEM), energy-dispersive X-ray spectroscopy (EDX), Raman spectroscopy, Fourier transform infrared spectroscopy (FTIR), and X-ray diffraction (XRD) were first employed to explore the morphology and composition of the hybrid gas-sensitive nanomaterial. To analyze the resultant nanomaterials, many methods were employed. The crystallinity of carbon nanotubes and the presence of In nanoparticles in the hybrid samples, for instance, were both determined by using Raman spectroscopy. For this investigation, a Raman spectrometer from Renishaw and a confocal Leica DM2500 microscope were connected. The Raman spectrometer carried out the operation with a laser at a wavelength of 532 nm.

The morphology of the hybrid nanomaterial was examined using a ZEISS Gemini 500 FESEM at a voltage of 30 kV. It is a high-resolution FESEM that can image nanoscale objects including wafers with a 100 mm diameter and tiny bits. It has exceptional resolution and picture clarity at both high and low accelerating voltages.

MWCNTs/In NPs have been formed on silicon substrate, and FTIR tests have been conducted in the 400 to 4000 cm^{-1} range to identify the functional groups of the In NPs.

3.1. Field Emission Scanning Electron Microscope (FESEM). The field emission scanning electron microscope validates the surface morphology of the produced samples, including nanoparticle distribution and size of the nanoparticle, and reveals the shape and structure of the nanoparticles linked to the MWCNTs. The FESEM (ZEISS Gemini SEM 500) allows for the acquisition of sample surface morphology at extremely high resolution. The FESEM micrographs of the samples as they were produced are displayed in Figure 3. As shown in the picture, the In nanoparticles connected to the MWCNTs are indicated by a cluster of luminescent bright spots. As the amount of deposition increases over time in each sample, the density of the spot cluster also increases. The density of the cluster demonstrates the binding of In nanoparticles to the MWCNT surface.

These nanotubes were subsequently decorated with indium nanoparticles, which can be seen as bright spots on the CNT surfaces. The micrographs show the high density of the linked nanoparticles as well as the relatively uniform distribution of nanoparticles on the surfaces of the CNTs. Because it is easy for metal nanoparticles to combine, NPs are conjugated with CNTs to get around problems with the stability, separation, and recovery of NPs as well as prevent their aggregation.

The figure displays SEM morphological micrographs of the MWCNT/In nanocomposite and the bare sample, each at a 200 nm magnification. Spread throughout the surface of the MWCNTs, nanoparticles have been proven to be useful. This illustrates that we may use a preprocessing step to produce a homogeneous deposition of the linked metal nanoparticles on MWCNTs. The carbon nanotube diameter dispersion is most frequently found between 45 and 55 nm.

3.2. Energy-Dispersive X-ray Spectroscopy (EDX). As shown in Figure 4, the purple dots represent the carbon concentration and the green spots represent the decoration of In nanoparticles; these reveal that In nanoparticles have been used to decorate multiwalled carbon nanotubes. The EDX spectrum also recognizes signals related to the element Fe, but we only need to display the amounts of carbon and In nanoparticles. The micrographs in the picture display the

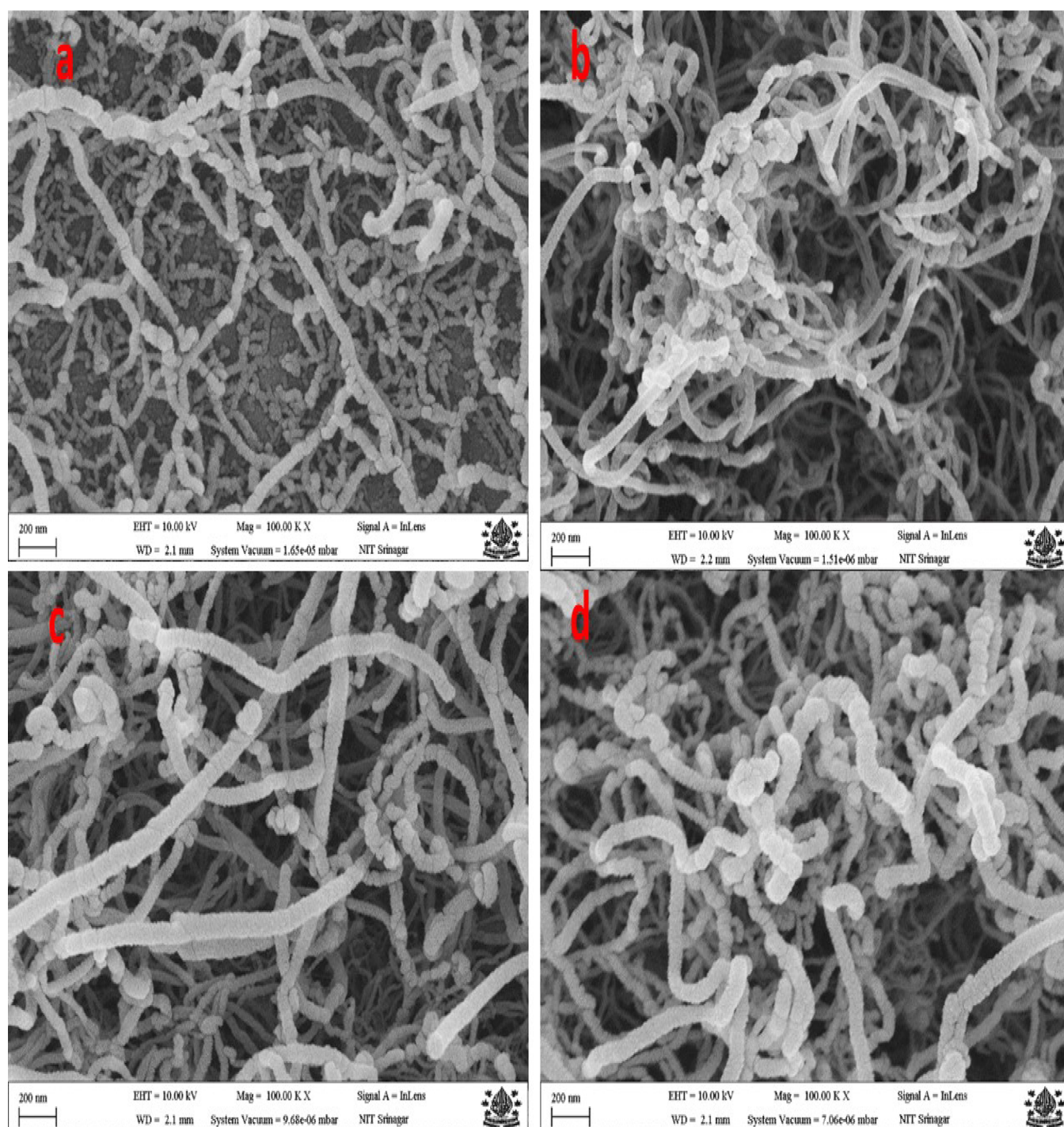


Figure 3. FESEM micrographs of (a) pristine and (b) to (d) decorated CNTs with In nanoparticles at different time intervals 3, 6, and 9 min, respectively.

concentration of carbon and indium metal nanoparticles used as decorations. The carbon signal is stronger in spectrum (a) than it is in all of the corresponding micrographs (b–d), shown in Figure 4, and the resolution of all the micrographs is 10 μm . Functionalization also improves the deposition of metal nanoparticles and metal oxides onto the MWCNTs for various purposes. Carboxylic acid, hydroxides, and other functional groups will be attached to the outer surface of the MWCNTs by the use of acid to functionalize them, serving as an anchor seed for the deposition of metal nanoparticles and metal oxides. In the EDX elemental maps, the produced sample of

MWCNT-In nanocomposites demonstrates that it has the carbon concentration and metal deposition concentration that are depicted in the maps, respectively.

3.3. Raman Spectroscopy. Utilizing Raman (Renishaw) spectroscopy, CNT quality was evaluated. The as-grown CNTs with iron catalysts were examined by using a Renishaw excitation laser beam with a 532 nm wavelength. The Raman spectra of the samples that were created using the low-pressure chemical vapor deposition technique are displayed in Figure 5. Silicon (Si) is the substrate that was utilized to make the sensing samples. Raman characteristics contain two prominent

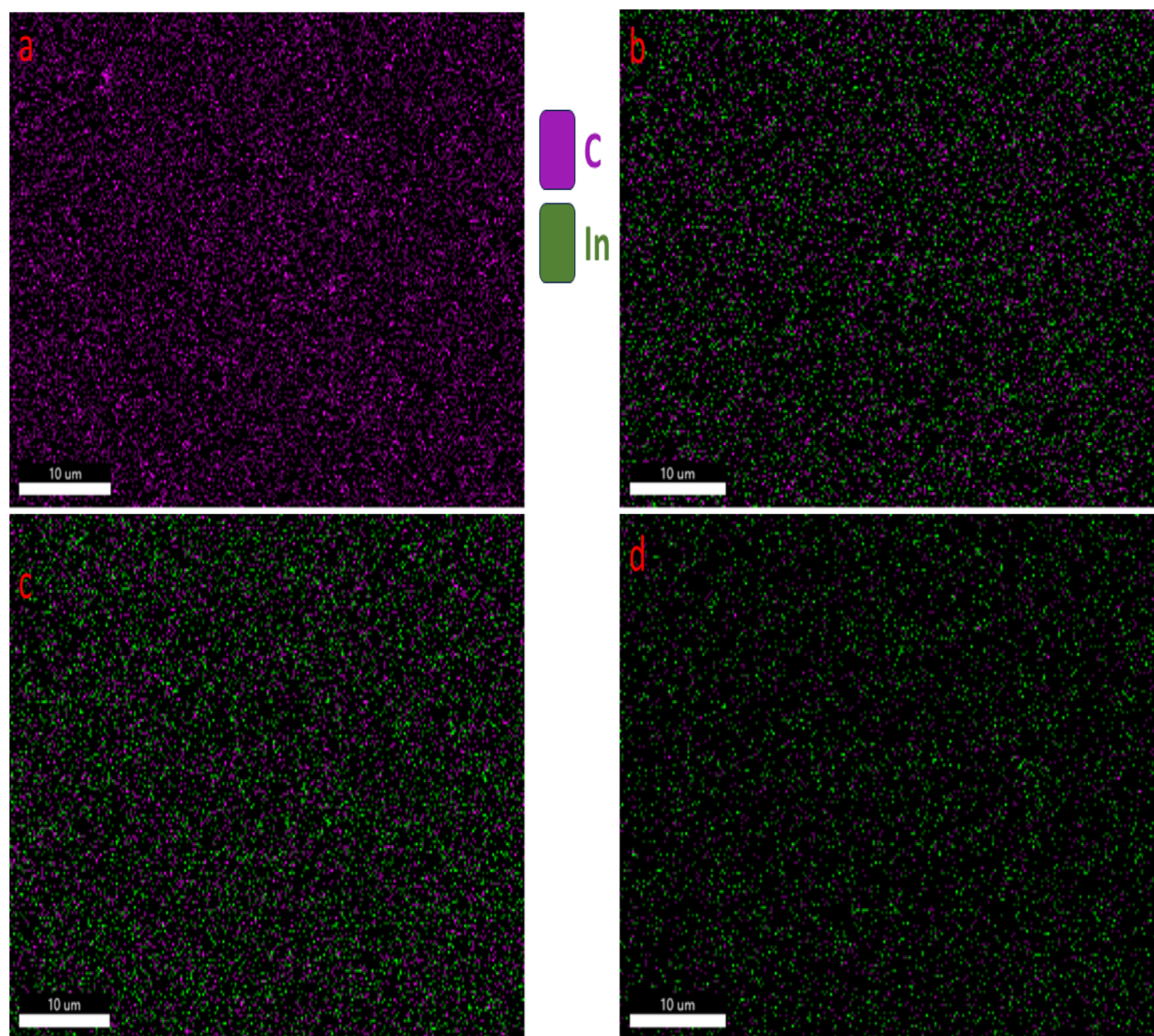


Figure 4. EDX elemental maps of (a) pristine and (b–d) decorated MWCNTs.

modes, namely, the radial breathing mode at low frequencies and the tangential G-band at specific frequencies, but the spectrum is devoid of the RBM ($100\text{--}300\text{ cm}^{-1}$) modes because we began the procedure at 400 cm^{-1} , which leads to the production of MWCNTs. The G-band, also known as the high-energy band in our study, arises at 1547 cm^{-1} in the pristine sample and represents the stretching mode of the graphite plane, which pertains to the dimensions $1500\text{ to }1600\text{ cm}^{-1}$. Defect-induced double-resonant decay produces the D-band, which has a wavelength between $1300\text{ and }1400\text{ cm}^{-1}$. In the pristine, there is D-band Raman scattering at 1342 cm^{-1} . A second-order two-phonon process with a substantial frequency dependency on the excitation laser energy, which has a wavelength range of $2500\text{--}2800\text{ cm}^{-1}$, is the G^1 -band, also known as the 2D band. In pristine, the G^1 -band is located at 2695 cm^{-1} , as can be seen in the spectrum above. The intensity ratio of the D-band to the G-band may be evaluated in order to evaluate the defective quality of MWCNTs with varied metal nanoparticle concentrations.

The intensity ratio of the D-band to the G-band can be used to assess the MWCNTs' defective quality. The D-band, G-band, G^1 -band, I_D/I_G ratio, and I_G^1/I_G ratios of pristine, 3 min

decorated, 6 min decorated, and 9 min decorated are given in Table 1.

3.4. Fourier Transform Infrared Spectroscopy (FTIR).

FTIR measurements in the $400\text{ to }4000\text{ cm}^{-1}$ range have been performed in order to determine the functional group of MWCNTs/In NPs that have been deposited on silicon substrates. The FTIR spectra of pure MWCNTs and MWCNTs/In composites are shown in Figure 6. It has been observed that the In nanoparticles' FTIR spectra can reveal potential interactions between their surface and MWCNT molecules. It has been demonstrated by comparing the FTIR spectra of MWCNTs/In and MWCNTs that several peaks produced by pure MWCNTs were replicated in the FTIR spectra of In nanoparticles and CNTs with minor differences in position and transmission band strength. The spectra of pure MWCNTs-NPs show a minor shift in the transmission band at $2946\text{ and }1747\text{ cm}^{-1}$, which is attributable to the C–H symmetric stretching vibration, to $2922\text{ and }1739\text{ cm}^{-1}$, illustrating the interaction between the MWCNT molecules and Mn nanoparticles. According to the literature review, the broad peak that formed in the ranges $3146, 3261, \text{ and }3464\text{ cm}^{-1}$ is linked to the O–H stretching vibration. C=C bonds

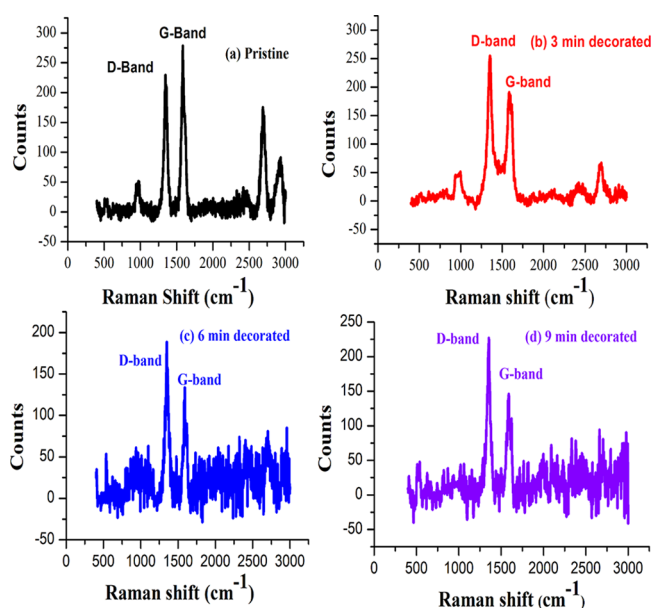


Figure 5. Raman spectra of the as-grown samples (a) pristine and (b, d) decorated MWCNTs.

Table 1. Various Parameters Obtained in the above Samples, Such as I_D/I_G and I_G^1/I_G

prepared samples	D-band (cm ⁻¹)	G-band (cm ⁻¹)	G ¹ -band (cm ⁻¹)	I_D/I_G	I_G^1/I_G
pristine MWCNT	1346	1584	2680	0.81	0.61
3 min In/MWCNT	1355	1587	2687	1.25	0.50
6 min In/MWCNT	1348	1590	2686	1.40	0.54
9 min In/MWCNT	1355	1591	2697	1.54	0.53

were discovered in aromatic rings with a carbon skeleton at 1636 cm⁻¹.

3.5. X-ray Diffraction. Crystallinity and other information, including crystal structure, orientation, and phase information, may be determined using XRD. Data was acquired between 20 and 80° at a scanning rate of 4 per minute. Cu K 1.5406 Å is the wavelength used for characterization. To verify the development of MWCNTs produced on a Si substrate, the peaks of 26.1, 26.2, and 26.0 were measured. In Figure 7, the XRD pattern of MWCNTs made with different metal concentration is displayed. The peaks of 37.3 and 66.05 verify the In metal decoration on the MWCNT sensor. Peak crystalline percentages can be calculated to a range of values between 20 and 80° of theta, from 25 to various values. Due to the erratic power of the RF magnetron, the surface of MWCNTs is altered as the deposition time increases potentially reducing crystallinity, when the quantity of metal nanoparticle decoration on the surface rises via the RF-sputtering process. The concentration of carbon reduces as the power increases. The proportion of crystallinity decreases as the number of In nano particles on the surface increases.

4. GAS SENSING STUDIES: RESISTANCE VARIATION

In this work, we developed a resistive-based gas sensor using MWCNTs as active sensing layers. The interaction of gas molecules with the detecting layer changed the electrical

resistance of the gas sensors used in this study, and the degree of this change was proportional to the type and concentration of the gas. The electrical resistive transduction mechanism served as the foundation of these sensors. Figure 8 displays the dynamic resistance curves for bare and In NP-decorated MWCNT sensors at the same NH₃ gas concentrations and ambient temperature. The resistance fluctuation magnitude of each pair of MWCNT sensors was also evaluated at the same NH₃ concentration level (10 ppm) and the same temperature (25 °C), with and without the gas being evacuated from the chamber. A limited recovery was seen in this case because the gas molecules are still stuck to the MWCNT sensor surface while the gas is left in the chamber. However, the pristine MWCNT sensor recorded a higher resistance change in kilohms, but the In-decorated MWCNT sensor displayed a larger resistance shift in mega-ohms; this distinction is seen in Figure 8. When the temperature is too low, there is not enough energy to overcome the adsorption barrier, preventing target gases from adhering to the sensor's surface properly. Additionally, when the operating temperature is high, the desorption rate will be greater than the adsorption rate, causing the responsiveness to drop. At the optimal sensing temperature, the rates of adsorption and desorption are identical and the target gas molecules have sufficient energy to overcome the adsorption barrier, producing a robust response. We had been working on the room temperature, which a preliminary test showed to be 25 °C. A Keithley 6514 source meter is linked to the computer, and data has been used.

4.1. Response Curves. Figure 9 illustrates the gas sensing response curves for various concentrations of In metal nanoparticles at various time intervals. The prepared pristine and embellished MWCNTs sensors were tested for NH₃ detection at room temperature, as can be seen from the response curves below. At 10 ppm of ammonia gas, the entire process was evaluated. The following formula was used to determine the size of the sensor response:

$$[(R_{\text{gas}} - R_{\text{air}})/R_{\text{air}}] \times 100$$

where R_{gas} denotes resistance of the sensor in the presence of the testing gas and R_{air} in the presence of the air gas mixture, respectively. The as-prepared samples had sensitivity values of 0.45, 0.50, 0.51, and 0.57, respectively. If we quantify the sensitivity as a percentage, the pristine sensor has a sensitivity of 45% whereas the other sensors have values of 50, 51, and 57%, respectively. For reducing gases and oxidizing gases, respectively, R_a/R_g and R_g/R_a were used to measure the sensors' sensitivity. The response curves in Figure 8 depict the acquired responses from the sensing layer. A high-quality sensor response of about 117% has been obtained in the pristine sample followed by responses of 144% in 3 min of decoration and approximately 115 and 73% in 6 and 9 min of decorated sensors, respectively.

We observed the fast response (1–10 s) in pristine and (1–7 s) in embellished samples. Using the resulting sensor response graph as a guide, 80–85% recovery was achieved. This clearly shows that the pure MWCNT sensor resistance was formed due to the reducing nature of NH₃ and that this resistance increased with the gas particle contact. The saturation state does, however, need to be improved because it reveals variations in the resistance on the sample's surface.

4.2. Selectivity of the Sensors. The appropriate selectivity toward a particular gas among other gases is the other quality of a good chemical resistive sensor. The

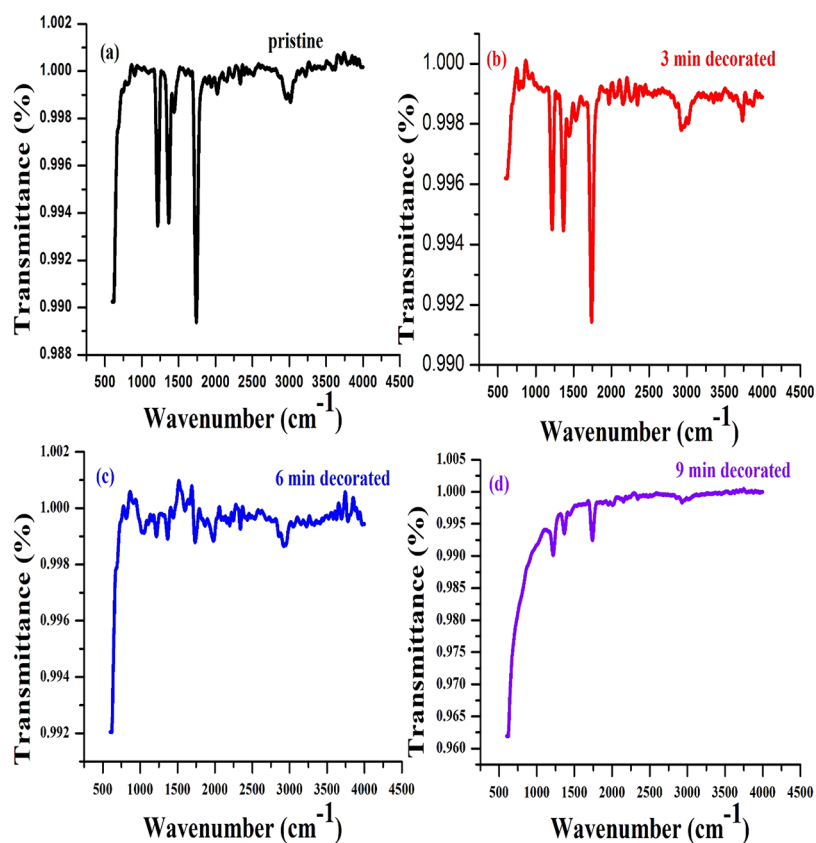


Figure 6. FTIR analysis of (a) bare MWCNT film and (b–d) decorated MWCNT films.

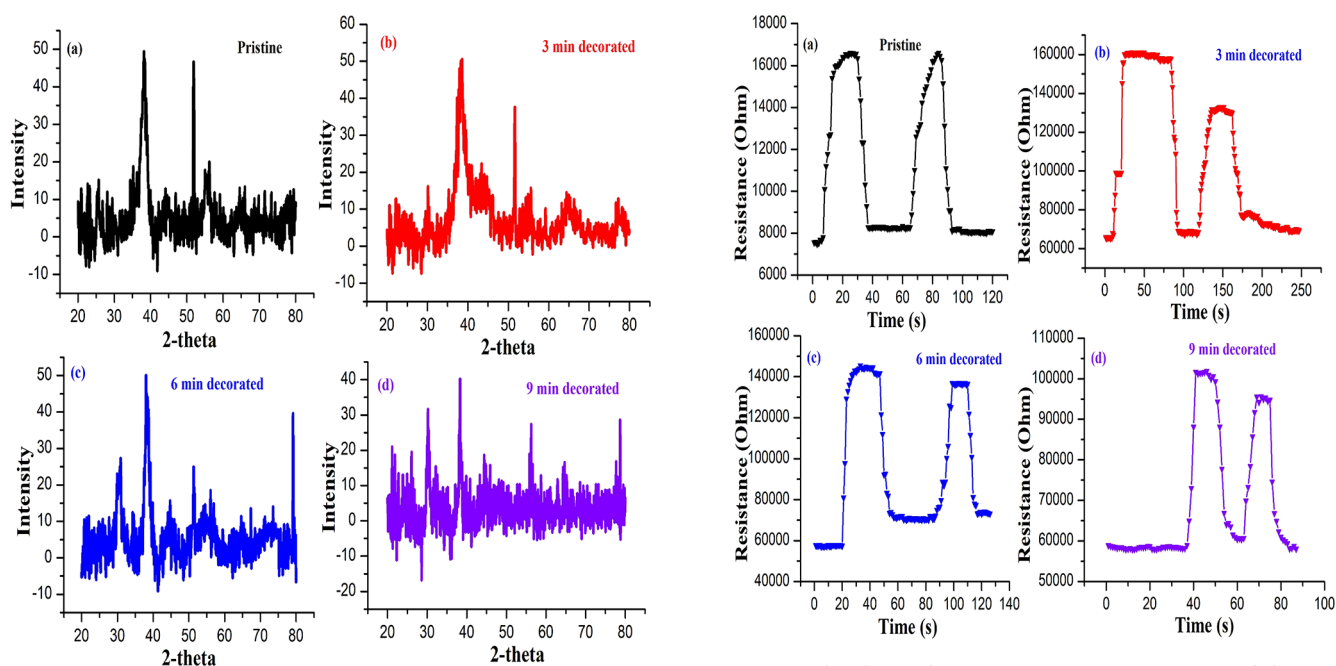


Figure 7. XRD pattern of the as-prepared MWCNT (a) pristine and (b, d) decorated sensors.

developed sets of MWCNT sensors in this case have been assessed for a range of compounds at fixed concentrations and temperatures (10 ppm and 25 °C, respectively). It has been shown that the as-fabricated MWCNT sensor is very selective for NH_3 in comparison to other gases based on response measurements of all other gases, including NO_2 , CO , and H_2 .

Figure 8. The electrical resistance variation in pristine and decorated prepared samples.

In the initial conditions, all other gases had sensor responses of less than 50%, as shown in Figure 10, whereas NH_3 recorded sensor responses of about 120%. The gas selectivity of the MWCNT and MWCNT/In sensors at 10 ppm for all four of the constructed gas sensors is shown in the bar diagram in Figure 10. It is evident that under given circumstances, the pristine sensor's sensitivity to NH_3 is 45%. Additionally, the 9

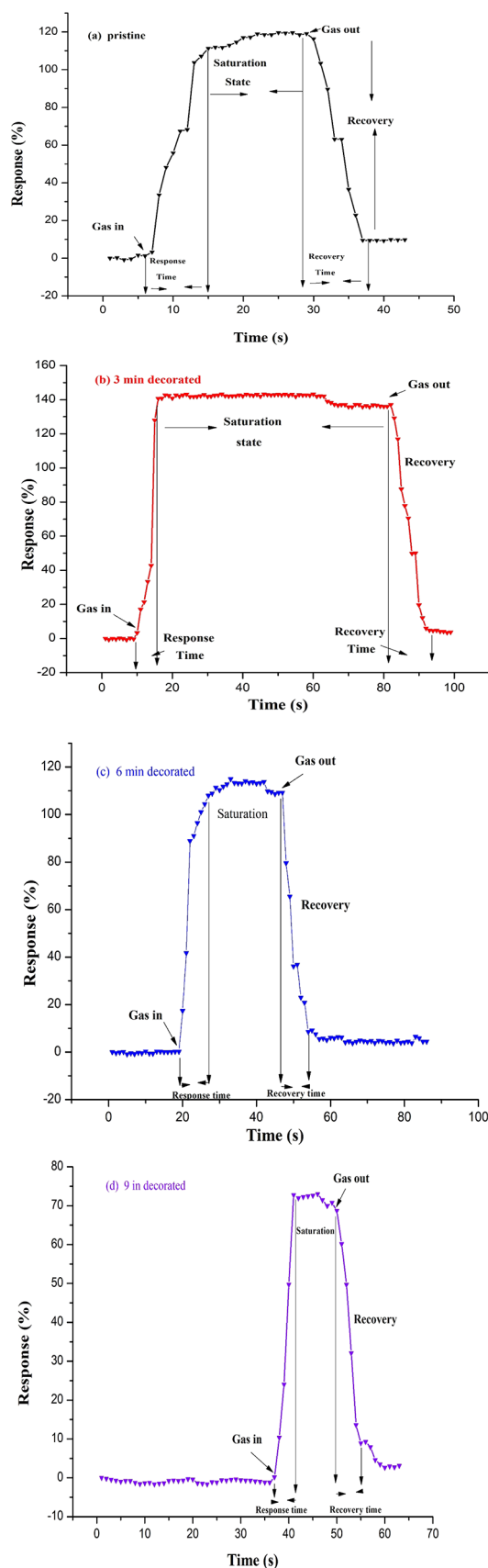


Figure 9. (a–d) Shows the sensor response curves toward the NH_3 gas detection at 10 ppm at room temperature.

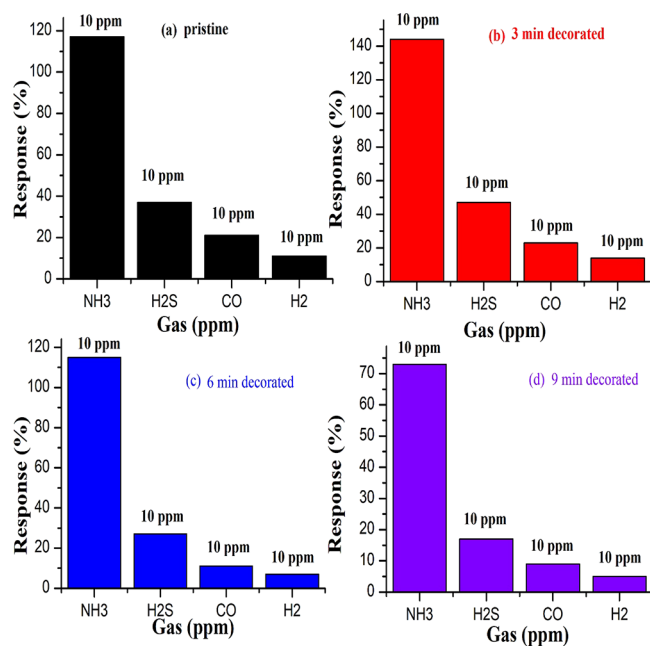


Figure 10. Measurements of the selectivity of pristine and (b–d) decorated MWCNT sensors.

min decorated sensor has the best reaction time of the four, with NH_3 having the maximum sensitivity (57%). The other three gases are considerably less sensitive than the rest of the samples. The sensor is shown to have better selectivity for NH_3 than that for H_2S , CO , and H_2 . While the responses for the other gases were low, the response for NH_3 was reported to be 144% in the case of the In-nanoparticle-decorated sensor set. In detail, the effect of In nanoparticles on MWCNTs is described properly because of the high affinity between NH_3 gas molecules and MWCNT surfaces. It is conclusively proven that there is considerable charge transfer; as a result, the sensor responsiveness is enhanced.

4.3. Concentration Effect on the Sensors. The sensor's reaction gets somewhat more sensitive as the gas concentration rises. For instance, when the gas concentration was increased to 70 ppm, the reaction was better. The response of the gas sensor increases in accordance with the rise in the gas concentration at different concentrations. When the gas concentration is changed by 10, 30, 50, and 70 ppm, the response curve rises sharply. As we raise the gas concentration of the target gas, as shown in Figure 11, the reaction curve increases.

4.4. Stability of the Sensors. Comparing embellished MWCNT sensors to bare CNT, the stability assessment is appropriate. In terms of stability and reaction, the comparison between the 3 min embellished MWCNT and the pristine one is outstanding. The decorated sensors exhibit greater long-term stability than the naked carbon nanotubes, as shown in Figure 12. Stability is another essential quality for a sensor to be used for a long time in industries. At a concentration of 10 ppm and room temperature, all of the sensors were tested. The stability of the sensors was assessed over the course of 7 days at regular intervals of 1 day each. The sensor is more responsive and stable throughout the course of the entire day with a steady gas concentration.

Since CNTs have such a good quality, they are regarded as a strong candidate among the carbonaceous materials. Gas

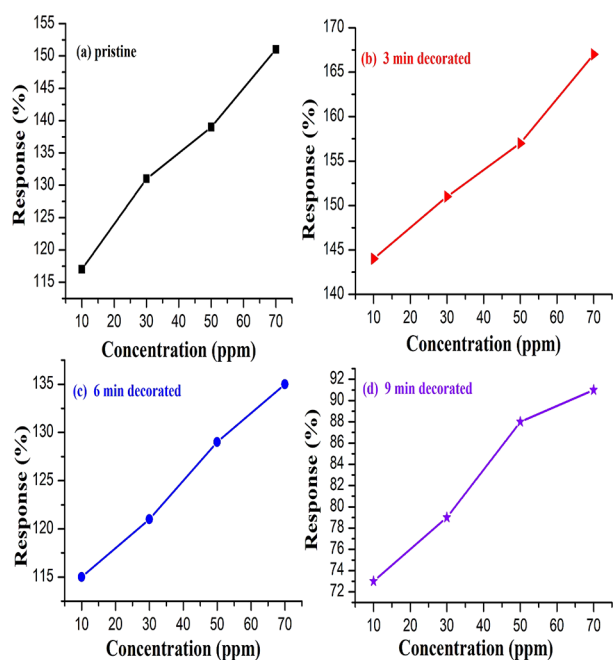


Figure 11. The response vs gas concentration in all sets of sensors.

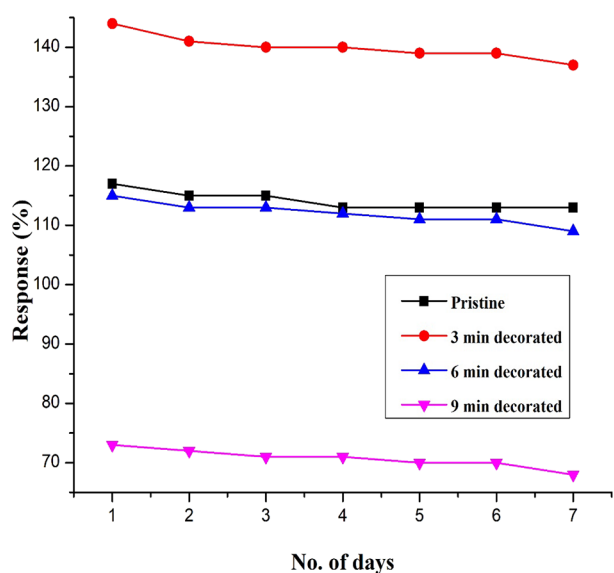


Figure 12. Stability measurement of MWCNT sensors at 10 ppm.

sensors are among the many possible applications for CNTs because of their special qualities as well as their distinct and compact structure. Furthermore, high-quality CNT sensors with various orientations are being fabricated in order to detect

NH_3 and other pollutant gases like CO_2 and NO_2 at trace-level concentration to monitor the environment properly. The higher the surface area, the larger the adsorption of target gas molecules, and hence the sensing response will be higher. Gas sensing properties are also largely dependent on CNT defect sites and surface phenomena. Table 2 shows the comparison between the materials from some previous literature.

5. CONCLUSIONS

In this work, low-pressure chemical vapor deposition was used to successfully fabricate gas-sensing devices based on conducting pristine MWCNTs, 3 min In-decorated MWCNTs, 6 min In-decorated MWCNTs, and 9 min In-decorated MWCNTs for ammonia detection purposes. The devices were then characterized under NH_3 exposure. Additionally, room-temperature measurements are made of our MWCNT and MWCNT/In ammonia gas sensors and the change in the electrical resistance curves and response curves is shown in Figures 8 and 9, respectively. Under a 10 ppm ambient ammonia gas concentration, the device's sensitivity rose from 45% in pristine CNTs to 57% in the 3 min In-nanoparticle-decorated sensor. In both unadorned and decorated MWCNTs, we have seen characteristics of a rapid reaction rate of (1–10 s) in pristine and (1–7 s) in decorated. Additionally, we have obtained responses of 117, 144, 115, and 73% in that order among all the four sensors, respectively. The sensitivity values for the samples as-prepared were 45% for the pure and 50, 51, and 57% for the remaining sensors. The measured sensor response graph showed that a recovery of 80 to 85% was attained. The stability was also evaluated during a 10-day period with a steady concentration given in Figure 12. The sensor has demonstrated an excellent response, increase in resistance, sensitivity, selectivity, stability, and recovery as well.

ASSOCIATED CONTENT

Data Availability Statement

The report that was provided contains all of the data that was compiled or examined during this investigation.

AUTHOR INFORMATION

Corresponding Author

Javid Ali – Material Science Lab, Department of Physics, Jamia Millia Islamia, New Delhi 110025, India; orcid.org/0000-0001-8042-8733; Email: javi_reslab@rediffmail.com, jali1@jmi.ac.in

Authors

Shah Masheerul Aalam – Material Science Lab, Department of Physics, Jamia Millia Islamia, New Delhi 110025, India

Table 2. Comparison table of some materials from previous literature

material	operating temp (°C)	concentration (ppm)	response (%)	response time (s)	recovery time (s)	ref.
graphene	RT	160	~8	~50	NA	40
ZnO thin film	150	600	~57	~120	~600	41
Cu-doped ZnO	RT	100	~30	13	33	42
ZnO nanoflakes	250	3	~80	3–15	5–14	43
$\text{TiO}_2/\text{Ti}_2\text{C}_3\text{T}_x$	RT	30	40.6	10–92	5–42	44
PANI/ NiCo_2O_4	RT	20	4.67	22	62	45
(MO_x) decorated graphene	RT	100–500	4.73	100–120	98–109	46
MWCNTs/In	RT	10	~144	~1–7	~1–10	this Work

Mohd Sarvar – Material Science Lab, Department of Physics, Jamia Millia Islamia, New Delhi 110025, India
Mohd Sadiq – Material Science Lab, Department of Physics, Jamia Millia Islamia, New Delhi 110025, India; A.R.S.D. College, University of Delhi, New Delhi 110021, India

Complete contact information is available at:

<https://pubs.acs.org/10.1021/acsomega.3c07244>

Author Contributions

S.M.A.: conceptualization, methodology, data curation, formal analysis, writing of the original draft, writing—review and editing. M.Sar.: visualization, validation, methodology. M.Sad.: visualization. J.A.: conceptualization, supervision, resources, writing—review and editing.

Notes

The authors declare no competing financial interest.

ACKNOWLEDGMENTS

We are all grateful to the National Institute of Technology's Centre for Research Facility (CRF) in Srinagar for providing characterization tools including FESEM, Raman, and XRD. We are also thankful to Miranda House (University of Delhi) for providing the sensing apparatus. I am also grateful to the Prime Ministers Research Fellowship (PMRF), which I got under the Lateral Entry Scheme in May Cycle 2022 under PMRF-ID, 3302523, that the Ministry of Higher Education (Govt. of India) awarded me.

REFERENCES

- (1) Chang, Y. W.; Oh, J. S.; Yoo, S. H.; Choi, H. H.; Yoo, K. H. Electrically refreshable carbon-nanotube-based gas sensors. *Nanotechnology* **2007**, *18* (43), No. 435504.
- (2) Lu, G.; Ocola, L. E.; Chen, J. Reduced graphene oxide for room-temperature gas sensors. *Nanotechnology* **2009**, *20* (44), No. 445502.
- (3) Zhang, T.; Mubeen, S.; Myung, N. V.; Deshusses, M. A. Recent progress in carbon nanotube-based gas sensors. *Nanotechnology* **2008**, *19* (33), No. 332001.
- (4) Radhakrishnan, J. K.; Kumara, M.; Geetika. Effect of temperature modulation, on the gas sensing characteristics of ZnO nanostructures, for gases O₂, CO and CO₂. *Sens. Int.* **2021**, *2*, No. 100059.
- (5) Tang, X.; Debliquy, M.; Lahem, D.; Yan, Y.; Raskin, J. P. A review on functionalized graphene sensors for detection of ammonia. *Sensors* **2021**, *21* (4), 1443.
- (6) Chen, M.; Wang, Z.; Han, D.; Gu, F.; Guo, G. Porous ZnO polygonal nanoflakes: synthesis, use in high-sensitivity NO₂ gas sensor, and proposed mechanism of gas sensing. *J. Phys. Chem. C* **2011**, *115* (26), 12763–12773.
- (7) Chowdhury, N. K.; Bhowmik, B. Micro/nanostructured gas sensors: The physics behind the nanostructure growth, sensing and selectivity mechanisms. *Nanoscale Advances* **2021**, *3* (1), 73–93.
- (8) Gaiardo, A.; Zonta, G.; Gherardi, S.; Malagù, C.; Fabbri, B.; Valt, M.; Vanzetti, L.; Landini, N.; Casotti, D.; Cruciani, G.; Della Ciana, M.; Guidi, V. Nanostructured SmFeO₃ gas sensors: Investigation of the gas sensing performance reproducibility for colorectal cancer screening. *Sensors* **2020**, *20* (20), 5910.
- (9) Chen, X.; Wong, C. K.; Yuan, C. A.; Zhang, G. Nanowire-based gas sensors. *Sens. Actuators, B* **2013**, *177*, 178–195.
- (10) Valt, M.; Fabbri, B.; Gaiardo, A.; Gherardi, S.; Casotti, D.; Cruciani, G.; Pepponi, G.; Vanzetti, L.; Iacob, E.; Malagù, C.; Bellutti, P.; Guidi, V. Aza-crown-ether functionalized graphene oxide for gas sensing and cation trapping applications. *Mater. Res. Express* **2019**, *6* (7), No. 075603.
- (11) Iijima, S. Helical microtubules of graphitic carbon. *nature* **1991**, *354* (6348), 56–58.
- (12) Mubarak, N. M.; Abdullah, E. C.; Jayakumar, N. S.; Sahu, J. N. An overview on methods for the production of carbon nanotubes. *Journal of Industrial and Engineering Chemistry* **2014**, *20* (4), 1186–1197.
- (13) Iijima, S.; Ichihashi, T. Single-shell carbon nanotubes of 1-nm diameter. *nature* **1993**, *363* (6430), 603–605.
- (14) Bethune, D. S.; Kiang, C. H.; De Vries, M. S.; Gorman, G.; Savoy, R.; Vazquez, J.; Beyers, R. Cobalt-catalysed growth of carbon nanotubes with single-atomic-layer walls. *Nature* **1993**, *363* (6430), 605–607.
- (15) Kumar, M.; Borah, P.; Devi, P. Methods including biomarkers used for detection of disinfection by-products. In *Disinfection By-Products in Drinking Water*; Butterworth-Heinemann, 2020 (pp 413–431)
- (16) Shaaban, H.; Mostafa, A.; Górecki, T. Green gas and liquid capillary chromatography. In *The Application of Green Solvents in Separation Processes*; Elsevier, 2017 pp 453–482
- (17) Tharsika, T.; Thanihachelvan, M.; Haseeb, A. S. M. A.; Akbar, S. A. Highly sensitive and selective ethanol sensor based on ZnO nanorod on SnO₂ thin film fabricated by spray pyrolysis. *Front. Mater.* **2019**, *6*, 122.
- (18) Zhu, X.; Zhang, J.; Xie, Q.; Hou, Z. L. High-sensitivity and ultrafast-response ethanol sensors based on graphene oxide. *ACS Appl. Mater. Interfaces* **2020**, *12* (34), 38708–38713.
- (19) Zhang, K.; Lin, Z. Highly sensitive ethanol sensor based on zinc oxide-based nanomaterials with low power consumption. *Journal of Materials Science: Materials in Electronics* **2021**, *32* (13), 17395–17405.
- (20) Saito, N.; Watanabe, K.; Haneda, H.; Sakaguchi, I.; Shimano, K. Highly sensitive ethanol gas sensor using pyramid-shaped ZnO particles with (0001) basal plane. *J. Phys. Chem. C* **2018**, *122* (13), 7353–7360.
- (21) Diao, Q.; Yin, Y.; Jia, W.; Xu, X.; Ding, Y.; Zhang, X.; Cao, J.; Yang, K.; Jiao, M. Highly sensitive ethanol sensor based on Ce-doped WO₃ with raspberry-like architecture. *Mater. Res. Express* **2020**, *7* (11), 115012.
- (22) Shan, H.; Liu, C.; Liu, L.; Wang, L.; Zhang, X.; Chi, X.; Bo, X.; Wang, K. Excellent ethanol sensor based on multiwalled carbon nanotube-doped ZnO. *Chin. Sci. Bull.* **2014**, *59*, 374–378.
- (23) Shooshtari, M.; Sacco, L. N.; Van Ginkel, J.; Vollebregt, S.; Salehi, A. Enhancement of room temperature Ethanol sensing by optimizing the density of Vertically Aligned Carbon Nanofibers decorated with gold nanoparticles. *Materials* **2022**, *15* (4), 1383.
- (24) Someya, T.; Small, J.; Kim, P.; Nuckolls, C.; Yardley, J. T. Alcohol vapor sensors based on single-walled carbon nanotube field effect transistors. *Nano Lett.* **2003**, *3* (7), 877–881.
- (25) Shaalan, N. M.; Hamad, D.; Saber, O. Co-Evaporated CuO-Doped In₂O₃ 1D-nanostructure for reversible CH₄ detection at low temperatures: Structural phase change and properties. *Materials* **2019**, *12* (24), 4073.
- (26) Shaalan, N. M.; Hamad, D.; Aljaafari, A.; Abdel-Latif, A. Y.; Abdel-Rahim, M. A. Preparation and characterization of developed CuxSn1-xO₂ nanocomposite and its promising methane gas sensing properties. *Sensors* **2019**, *19* (10), 2257.
- (27) Peng, N.; Zhang, Q.; Chow, C. L.; Tan, O. K.; Marzari, N. Sensing mechanisms for carbon nanotube based NH₃ gas detection. *Nano Lett.* **2009**, *9* (4), 1626–1630.
- (28) Zhang, J.; Boyd, A.; Tselev, A.; Paranjape, M.; Barbara, P. Mechanism of NO₂ detection in carbon nanotube field effect transistor chemical sensors. *Appl. Phys. Lett.* **2006**, *88* (12), 123112.
- (29) Kotarski, M.; Smulko, J. Noise measurement setups for fluctuations enhanced gas sensing. *Metrol. Measurement Syst.* **2009**, *16*, 457–464.
- (30) KOTARSKI, M. M.; SMULKO, J. M. Hazardous gases detection by fluctuation-enhanced gas sensing. *Fluctuation Noise Lett.* **2010**, *9* (04), 359–371.
- (31) Morrison, S. R. Selectivity in semiconductor gas sensors. *Sensors and actuators* **1987**, *12* (4), 425–440.

- (32) Yamazoe, N.; Shimanoe, K. Theoretical approach to the gas response of oxide semiconductor film devices under control of gas diffusion and reaction effects. *Sens. Actuators, B* **2011**, *154* (2), 277–282.
- (33) Zaretskiy, N. P.; Menshikov, L. I.; Vasiliev, A. A. On the origin of sensing properties of the nanostructured layers of semiconducting metal oxide materials. *Sens. Actuators, B* **2012**, *170*, 148–157.
- (34) Kharisov, B. I.; Kharissova, O. V.; Ortiz Mendez, U.; De La Fuente, I. G. Decoration of carbon nanotubes with metal nanoparticles: Recent trends. *Synthesis and Reactivity in Inorganic, Metal-Organic, and Nano-Metal Chemistry* **2016**, *46* (1), 55–76.
- (35) Lu, C. C.; Alshahrani, T.; Wu, R. J.; Fegade, U.; Jethave, G.; Al-Ahmed, A.; Khan, F.; Kolate, S. Synthesis of CeO₂–BiVO₄ nano photocatalyst material and used for the degradation of gaseous formaldehyde. *Opt. Mater.* **2023**, *144*, No. 114310.
- (36) Zhou, D.; Kang, Z.; Liu, X.; Yan, W.; Cai, H.; Xu, J.; Zhang, D. High sensitivity ammonia QCM sensor based on ZnO nanoflower assisted cellulose acetate-polyaniline composite nanofibers. *Sens. Actuators, B* **2023**, *392*, No. 134072.
- (37) Fegade, U.; Alshahrani, T.; Wu, R.; Lin, F.; Chang, X.; Yuan, S.; Al-Ahmed, A.; Khan, F.; Haq, B.; Afzaal, M. High-Selectivity Hydrogen Gas Sensors based on Mesoporous PbO_x-ZnO Nanocomposites. *Chem. - Asian J.* **2023**, No. e202300575.
- (38) Norizan, M. N.; Moklis, M. H.; Ngah Demon, S. Z.; Halim, N. A.; Samsuri, A.; Mohamad, I. S.; Knight, V. F.; Abdullah, N. Carbon nanotubes: Functionalisation and their application in chemical sensors. *RSC Adv.* **2020**, *10* (71), 43704–43732.
- (39) Mittal, M.; Kumar, A. Carbon nanotube (CNT) gas sensors for emissions from fossil fuel burning. *Sens. Actuators, B* **2014**, *203*, 349–362.
- (40) Mackin, C.; Schroeder, V.; Zurutuza, A.; Su, C.; Kong, J.; Swager, T. M.; Palacios, T. Chemiresistive graphene sensors for ammonia detection. *ACS Appl. Mater. Interfaces* **2018**, *10* (18), 16169–16176.
- (41) Li, C. F.; Hsu, C. Y.; Li, Y. Y. NH₃ sensing properties of ZnO thin films prepared via sol–gel method. *J. Alloys Compd.* **2014**, *606*, 27–31.
- (42) Mhlongo, G. H.; Shingange, K.; Tshabalala, Z. P.; Dhonge, B. P.; Mahmoud, F. A.; Mwakikunga, B. W.; Motaung, D. E. Room temperature ferromagnetism and gas sensing in ZnO nanostructures: Influence of intrinsic defects and Mn, Co, Cu doping. *Appl. Surf. Sci.* **2016**, *390*, 804–815.
- (43) Kanaparthi, S.; Govind Singh, S. Highly sensitive and ultra-fast responsive ammonia gas sensor based on 2D ZnO nanoflakes. *Mater. Sci. Energy Technol.* **2020**, *3*, 91–96.
- (44) Zhang, D.; Yu, S.; Wang, X.; Huang, J.; Pan, W.; Zhang, J.; Meteku, B. E.; Zeng, J. UV illumination-enhanced ultrasensitive ammonia gas sensor based on (001) TiO₂/MXene heterostructure for food spoilage detection. *J. Hazard. Mater.* **2022**, *423*, No. 127160.
- (45) Zhang, D.; Yang, Y.; Xu, Z.; Wang, D.; Du, C. An eco-friendly gelatin based triboelectric nanogenerator for a self-powered PANI nanorod/NiCo₂O₄ nanosphere ammonia gas sensor. *Journal of Materials Chemistry A* **2022**, *10* (20), 10935–10949.
- (46) Zhang, D.; Liu, J.; Jiang, C.; Liu, A.; Xia, B. Quantitative detection of formaldehyde and ammonia gas via metal oxide-modified graphene-based sensor array combining with neural network model. *Sens. Actuators, B* **2017**, *240*, 55–65.